Intertwined magneto-optical and plasmonic effects in Ag/Co/Ag layered structures

Elías Ferreiro-Vila, Juan B. González-Díaz, Rui Fermento, María U. González, Antonio García-Martín, José M. García-Martín, Alfonso Cebollada, and Gaspar Armelles
Instituto de Microelectrónica de Madrid (IMM-CNM-CSIC), Tres Cantos, 28760 Madrid, Spain

David Meneses-Rodríguez and Emilio Muñoz Sandoval
Advanced Materials Department, IPICYT, Camino a la presa San José 2055, San Luis Potosí 78216, Mexico
(Received 15 July 2009; revised manuscript received 26 August 2009; published 30 September 2009)

Surface plasmon polariton (SPP) excitation effects on the magneto-optical (MO) activity of Au capped Ag/Co/Ag trilayers are studied as a function of Co thickness. An enhancement of the transverse MO Kerr signal under SPP excitation as compared with that obtained without SPP excitation is measured with a maximum value of 150 times obtained for the trilayer with 8 nm Co. Such enhancement on the magneto-optical activity due to SPP excitation is also five times higher than that obtained in Au/Co/Au trilayers in similar conditions. The lower optical absorption in the studied range and the sharper plasmon resonance of Ag vs Au are responsible for these values. On the other hand, magnetic field-induced SPP wavevector modulation $(\Delta k/k)_{SPP}$ is studied for these trilayers and compared both with previous results in the Au/Co/Au system as well as with the theory. In the wavelength considered here, the obtained values are similar for both Ag- and Au-based structures and on the order of 10^{-4}, pinpointing the role of the magnetic layer on the SPP wavevector modulation.

DOI: 10.1103/PhysRevB.80.125132 PACS number(s): 78.20.Ls, 73.20.Mf, 78.66.Bz

I. INTRODUCTION AND MOTIVATION

It is well known that at the interface between two media with dielectric constants of opposite sign, such as a metal and a dielectric, it is possible to excite electromagnetic waves named surface plasmon polaritons (SPPs).[1–3] Due to their specific properties, there has been an increasing interest in the last years in the development of applications based on these waves, constituting the field commonly denoted as plasmonics. On the one hand, SPP characteristics are strongly dependent on the optical properties of both metal and dielectric media, which makes them useful for the development of biological sensors.[4–6] On the other hand, SPP modes are evanescent waves strongly bounded to the metal-dielectric interface with the potential to overcome the light diffraction limit and therefore they become suitable candidates for light guiding at the subwavelength scale[7–9] or for super resolution far-field optical microscopy.[10,11]

One step further in the progress of plasmonics is associated with the development of active plasmonic devices, that is, the realization of materials combinations or configurations that allow the control of SPP properties by an external agent.[12–14] An interesting option for being used as SPP external control agent is the magnetic field.[15,16] The magnetic field ability to affect the properties of surface-plasmon polaritons in highly doped InSb semiconductors has been known for a long time.[17] This effect is governed by the nondiagonal elements of the dielectric tensor, ε_{ij}, responsible for the magneto-optical (MO) activity and whose value is controlled by the magnetic field, which in this kind of semiconductors turns out to be relatively high under the presence of moderate magnetic fields. However, for noble metals (such as gold and silver), the ones usually employed in plasmonics, extremely high magnetic fields (tens of Tesla) would be needed to obtain ε_{ij} elements with a sizeable value, and therefore enough SPP modulation properties. Ferromagnetic metals, on the contrary, possess large MO activity associated with their magnetization and could be suitable elements for active plasmonics. Nevertheless, ferromagnetic metals present an important drawback in their high absorption, which implies that the associated plasmon resonances are too broad and the propagation losses happen to be too high. A feasible way to reduce such damping without losing MO activity is to combine noble and ferromagnetic metals, forming what we denote as a magnetoplasmonic system.

When a plasmonic material is combined with a MO active one, both the plasmonic and the MO properties of the resulting magnetoplasmonic system become interrelated. For example, in the Au/Co/Au system, the MO activity can be greatly enhanced when the SPP resonance is excited:[16,18–21] in this situation the light absorption is maximum and, for specific layer thickness, the electromagnetic field of the light is greatly enhanced at the MO active layer (Co in this case). This leads, respectively, to a reduction in the system reflectivity and to an enhancement in the magnetic component of the MO activity[16,22] which altogether are responsible of the enhanced global MO response. Moreover, it has also been demonstrated that the SPP wavevector in Au/Co/Au trilayers can be modified by an external magnetic field due to its dependence with the off-diagonal elements of the dielectric tensor, which in turn are magnetic field dependent in these systems.[16]

Most of the previous studies have been done by using Au as the plasmonic component of the magnetoplasmonic material. However, compared to gold, silver exhibits narrower and more intense plasmon resonances in the visible range due to its lower absorption losses and its higher plasma-frequency value.[23,24] This makes silver an even better material candidate for the implementation of magnetoplasmonic materials, for instance, in sensing and telecom applications. However, the long-term chemical instability of silver represents a serious drawback against the actual realization of

these devices. For example, drastic changes in the SPP resonance of Ag layers due to the formation of Ag_2S over the Ag thin film exposed to room air have been reported.[25] To avoid this, a thin layer of a protecting material must be deposited on top of the Ag film as a capping layer, preventing Ag from deteriorating and therefore leading to a multilayer magnetoplasmonic system with improved plasmonic properties associated with the Ag presence. This approach has already been analyzed in the literature in the context of biosensors.[26] Directly dealing with magnetoplasmonic structures, a first attempt was carried out using Pt as capping layer of Ag/Co/Ag structures, but the high optical absorption of Pt and its poor protective performance against oxidation lead to modest MO activity enhancement values.[27] Obviously the best choice for capping layer would be a material with both good plasmonic properties and chemical stability, for which Au is one of the best candidates.

In this work we present a systematic study of the properties of Au capped Ag/Co/Ag trilayers grown by magnetron sputtering. Au and Ag layers thicknesses are maintained constant while the Co layer thickness is varied between 2 and 11 nm. Two main goals are sought. On one hand, to study the influence that surface-plasmon excitation has on the MO activity of Au capped Ag/Co/Ag trilayers as a function of Co thickness and compare it with previous results obtained for the Au/Co/Au system, therefore exploring the effect of substituting Au by Ag as plasmonic material. On the other hand, to study the modification in SPP wavevector (k_{SPP}) by the application of an external magnetic field due to the presence of a ferromagnetic counterpart in the structure. To reach these objectives, we have also performed a detailed characterization of the morphology, magnetic, optical, and magneto-optical properties of the fabricated structures.

II. EXPERIMENTAL AND THEORETICAL METHODS

Sample growth by dc magnetron sputtering was carried out in an ultrahigh-vacuum chamber with base pressure in the middle 10^{-9} mbar range. A series of 5 029909nm Au/5 nm Ag/X nm Co/7 nm Ag structures with Co thickness varying between 0 and 11 nm has been grown at room temperature (RT) over microscope slide glass (BK7) substrates. Additional structures, namely, 20 nm Au/Glass, 10 nm Au/20 nm Ag/Glass, and 10 nm Au/20 nm Co/Glass, were grown under the same conditions to extract the optical constants of Au, Ag, and Co. Prior to deposition, the glass substrates were ultrasound cleaned during 10 min in successive baths of deionized water, acetone and isopropanol. The substrates were outgassed at 150 °C for 30 min and then let cool down to RT for deposition. Deposition powers of 20 W (Au and Co) and 100 W (Ag) were applied to the targets, and the Ar pressures were 1×10^{-3} mbar for Au, 3×10^{-3} mbar for Ag, and 6.6×10^{-3} mbar for Co deposition, yielding deposition rates of 12, 10, and 2.8 nm/min, respectively.

The surface morphology of the fabricated structures was characterized by atomic force microscopy (AFM). AFM images were taken using a Nanotec™ microscope operating in noncontact dynamic mode, i.e., with a mechanically modulated cantilever. Silicon cantilevers from NanoSensors™ with a force constant $k=5$ N/m and tip radius of 10 nm were used.

Magnetic hysteresis loops at room temperature with magnetic field applied both in-plane and out-of-plane were obtained by Kerr measurements in transverse and polar configurations, respectively. The transverse Kerr loops were recorded by using a linearly polarized 532 nm (solid-state laser) light beam at 45° incidence angle geometry with the applied magnetic field in the film plane but perpendicular to the plane of incidence and measuring the variations in the reflected light intensity. In the case of the polar Kerr loops, linearly polarized 530 nm light at normal incidence was used with the magnetic field applied perpendicularly to the film plane, and the Kerr rotation angle and ellipticity of the elliptically polarized reflected light were measured.

Reflectivity (R) and transverse magneto-optical Kerr effect ($\Delta R/R$) curves in presence of plasmon excitation were also measured with a p-polarized HeNe laser and the sample mounted on a glass prism in Kretschmann configuration.[28] The magnitude $\Delta R/R$ is defined as

$$\frac{\Delta R}{R} \equiv \frac{R_{pp}(+H) - R_{pp}(-H)}{R_{pp}(+H) + R_{pp}(-H)}, \tag{1}$$

where $R_{pp}(+H)$ and $R_{pp}(-H)$ stand for the reflectivity (both incident and reflected light being p polarized) for maximum positive and negative applied field, respectively. The different elements of the dielectric tensor of the system (diagonal or purely optical as well as nondiagonal or magneto-optical) were obtained via combined spectral ellipsometry and Kerr effect measurements. Ellipsometry measurements taken with a M200FI J. A, Woollam Co.™ ellipsometer between 245 nm and 1.69 μm, and with angles of incidence ranging from 45° to 75° allowed extracting both real and imaginary parts (ε_1^{xx} and ε_2^{xx}, respectively) of the diagonal elements of the dielectric tensor. Polar Kerr spectra[29]were measured between 290 and 840 nm with a maximum magnetic field of 1.6 T, to ensure that the sample magnetization is fully saturated. From the polar Kerr spectra, and knowing the diagonal elements of the dielectric tensor of the system, the real and imaginary parts of the nondiagonal elements (ε_1^{xy} and ε_2^{xy}, respectively) can be calculated. Note here that our layers are polycrystalline without any preferred orientation and therefore we assume that the nondiagonal dielectric tensor elements are the same for all directions ($\varepsilon^{xy}=\varepsilon^{xz}=\varepsilon^{yz}$). Simulations of the MO Kerr signal, with and without SPP excitation for such structures, were performed via transfer-matrix method using the actual dielectric tensor elements of the materials obtained from ellipsometric and polar Kerr spectra.

III. RESULTS

Here we first present the results dealing with the morphological, magnetic, optical, and MO characterization of the fabricated structures, necessary to understand the SPP effect on the MO activity of these systems, and the magnetic field effects on the SPP wavevector, presented in the second part of this section.

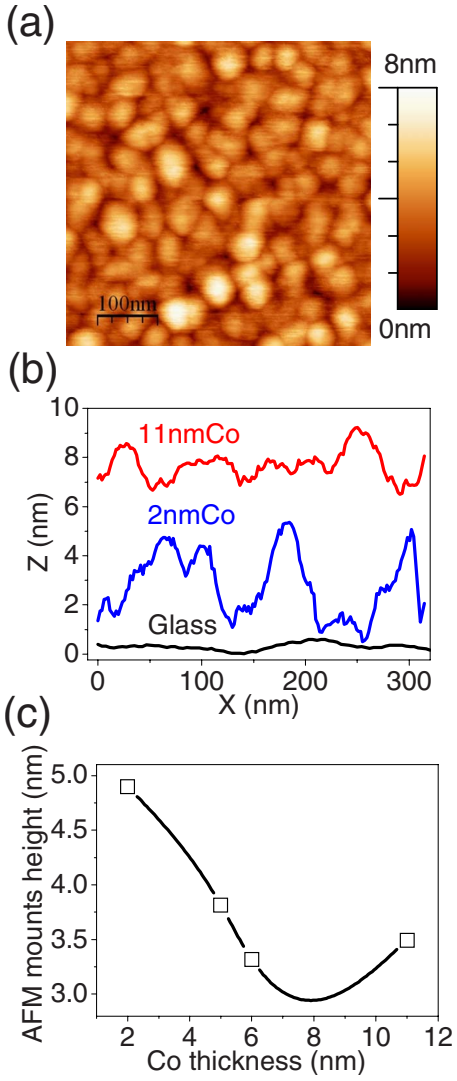

FIG. 1. (Color online) (a) AFM image of the 5 nm Co thick sample. (b) AFM profiles of two Au/Ag/Co/Ag multilayers with 2 and 11 nm Co thickness, respectively. The topographic profile of a glass substrate is also included as a reference. (c) Evolution of the mounts height with the Co thickness.

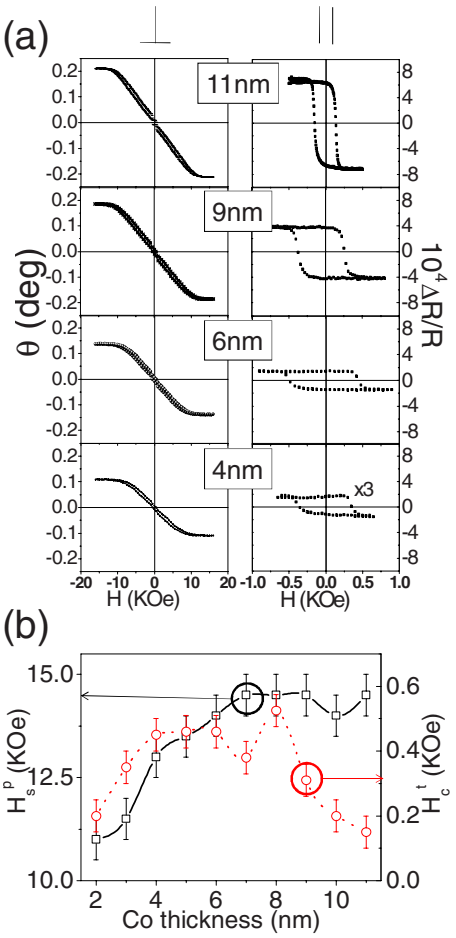

FIG. 2. (Color online) (a) Kerr loops of some representative samples (4–6 and 9–11 nm Co thicknesses) measured in polar (left side of the figure) and transversal (right side of the figure) configuration. (b) Evolution of the polar saturation field and the transverse coercivity with Co thickness.

A. Characterization

1. Morphology

The morphology of the samples has been analyzed by AFM, a representative image is shown in Fig. 1(a). Mounds are clearly observed in the sample surface. The lateral size of the mounds is similar (typical width around 50 nm) for all the samples, but their height decreases as the Co thickness increases, as shown in Fig. 1(b) for two representative topographic profiles corresponding to samples with 2 and 11 nm Co thickness. The profile of the glass substrate is also included as a reference. The substrate is rather flat, with 0.3 nm rms roughness, whereas the samples exhibit a deviation from ideal 2D growth, with mounds whose height varies from 5 nm for the 2 nm Co sample, down to 3.5 nm for the 11 nm Co one. Figure 1(c) shows the evolution of the average height of the mounds as a function of the Co thickness. For low Co thickness, the height is rather constant. At 6 nm Co thickness a sudden decrease is observed and above such value the mound height continues decreasing although at a lower rate. Taking into account that all the samples have the same layers on top of the Co one, it can be assumed that the initial mound height is mainly due to the first Ag layer grown over the glass substrate and that Co grows preferentially onto the valleys. When the Co thickness reaches 5 nm, the actual surface is now flatter and a continuous Co thin film can be formed: as a result, the final height of the structures is notably decreased.

2. Magnetic characterization

Kerr hysteresis loops in polar and transverse configurations (sensitive to out-of-plane and in-plane magnetization, respectively) have been measured for all the samples. Figure 2(a) shows the polar (left) and transverse (right) loops of representative samples. As expected, the MO signals (rotation angle in the polar configuration, changes in the reflected light intensity in the transverse one) increase with the Co amount. At a first glance, from the low saturation field and the high remanent magnetization for the transverse loops,

compared with the high saturation field and low remanent magnetization for the polar ones, an in-plane magnetic anisotropy can be deduced for all the samples. More relevant information can be obtained by analyzing the evolution with the Co thickness of two of those properties, as depicted in Fig. 2(c): the *polar* saturation field H_s^p and the *transverse* coercivity H_c^t. For low Co thickness, H_s^p monotonously increases until 7 nm; above such value, it is almost constant. Taking into account the aforementioned assumption that Co preferentially grows in the valleys of the rough Ag surface, such evolution can be explained as follows: for low thickness, the Co layer is not continuous but formed of mainly disconnected islands. The applied magnetic field must overcome the demagnetizing field in the perpendicular direction of those islands to saturate them. As the thickness increases, some islands become connected and their effective demagnetizing field increases (the ratio between their lateral dimensions and their height increases). Finally, when all the islanded regions coalesce, a continuous thin film of Co is formed, so the demagnetizing field reaches a maximum value and does not change for increasing thickness in the nm range: as a result, H_s^p saturates. It must be noticed that such continuous Co film is rough and as a consequence the maximum H_s^p is lower than that expected for a completely flat thin film (17 kOe). Such explanation can also account for the evolution of H_c^t. Once the continuous Co film is formed, the magnetization reversal for in-plane field takes place by domain-wall nucleation and propagation. With increasing thickness above 7 nm, the continuous film becomes more homogeneous: the number of pinning points for the domain-wall movement decreases and as a result H_c^t decreases.

Finally, we would like to mention that the magnetic field needed to saturate the samples in the transverse configuration, which is the one used for SPP wave-vector modulation as will be shown in Sec. III B 2, is lower than 0.75 kOe (75 mT), a very easily achievable value for the characterization as well as for the development of applications.

3. Optical and magneto-optical characterization

As the optical and magneto-optical properties of thin metal layers are influenced by the growth conditions, we have extracted the dielectric constants of our films by means of spectroscopic ellipsometry and polar Kerr spectroscopy. The optical constants of Au, Ag, and Co and magneto-optical constants of Co were obtained from 20-nm-thick layers grown on glass substrates, where the Ag and Co were capped with a 10 nm Au protective film to avoid oxidation. First, the 20 nm Au/Glass thin film was characterized by spectroscopic ellipsometry, its experimental optical constants being then used for the determination of those of the Au capped Ag and Co layers. In Fig. 3 we show real and imaginary parts of the diagonal elements of the dielectric tensor determined in this way for (a) Au, (b) Ag, and (c) Co. Figure 3(d) shows the magneto-optical constants of Co (real and imaginary parts), obtained from the experimental polar Kerr spectra of the mentioned 20 nm Co/Glass thin film.

Next, spectral MO characterization of the Au-capped Ag/Co/Ag trilayers was carried out. In Figs. 4(a) and 4(b) we show polar Kerr rotation (θ) and ellipticity (φ) spectra for

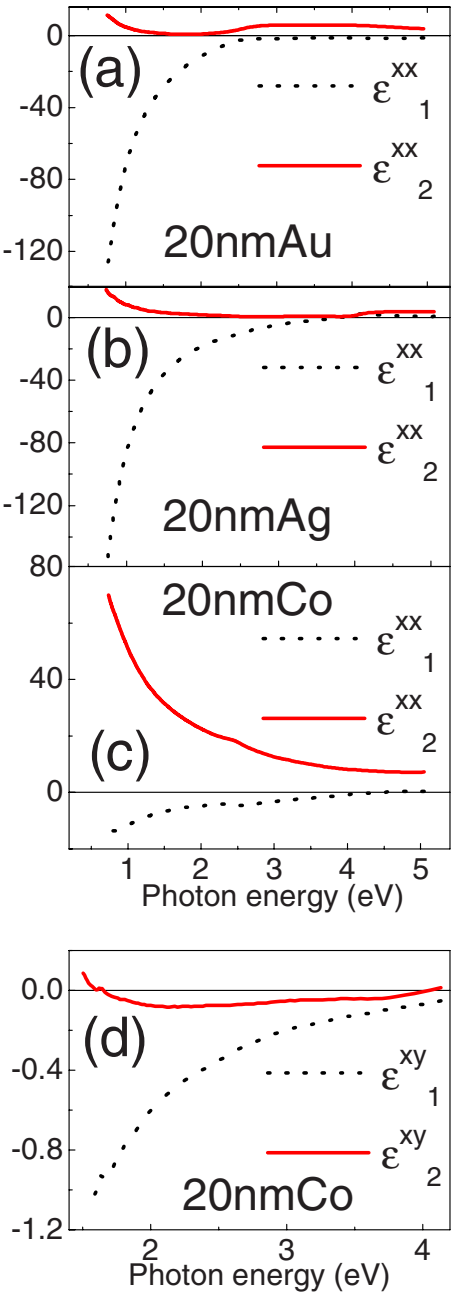

FIG. 3. (Color online) Optical constants and magneto-optical constants (real part ε_1 and imaginary part ε_2) of the metals composing the multilayers analyzed in this work, obtained by ellipsometric (optical constants) and polar Kerr (MO constants) spectra: (a) Au; (b) Ag; (c) Co; and (d) MO constants of Co. All the data have been extracted from 20-nm-thick films. In the case of Ag and Co, they were covered by a 10 nm Au layer to prevent oxidation.

representative samples (11, 8, 5, and 2 nm Co). As expected, a gradual increase in the overall MO activity with Co amount is observed. The minimum of the Kerr rotation roughly corresponds to the Co plasmon position. The overall behavior of both Kerr rotation an ellipticity is well reproduced by a theoretical calculation based on continuous layers with sharp interfaces (Fig. 5), where the used optical and MO constants are those experimentally obtained from the 20-nm-thick layers (see Fig. 3). However, the agreement is much better in

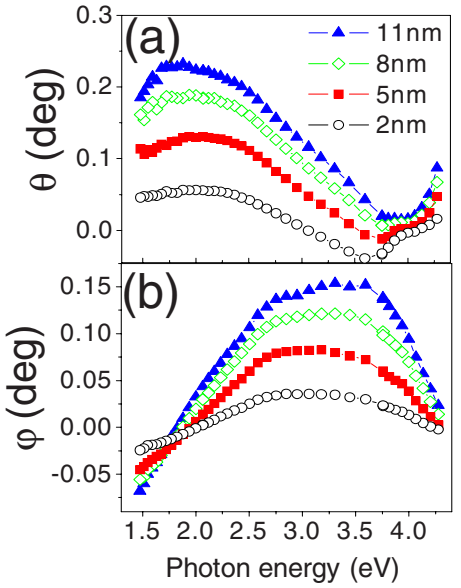

FIG. 4. (Color online) (a) Rotation and (b) ellipticity spectra of the Au/Ag/Co/Ag layers for four representative values of Co thickness: 2, 5, 8, and 11 nm.

the visible range, where the Kerr rotation roughly scales with the amount of Co, than in the UV range. In particular, the dip in the rotation at around 3.7 eV for the thinnest Co layer is not well captured. To understand the origin of this dip and the overall disagreement between theory and experiment in the UV range, we have to keep in mind that the layers have certain roughness, implying that for low Co thickness the layer continuity may be lost and therefore a continuous layer

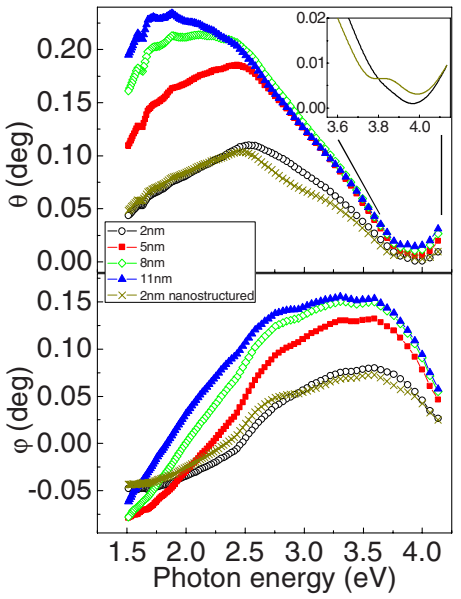

FIG. 5. (Color online) Theoretical Kerr rotation and ellipticity spectra for continuous Au/Ag/Co/Ag films for the same Co thicknesses as in Fig. 4 (symbols) and a nanostructured (Co islands on an Ag matrix) thin film (crosses) to estimate the effect of the layers continuity loss. The inset focuses on the high-energy region for the continuous and nanostructured film with the same Co amount (2nm).

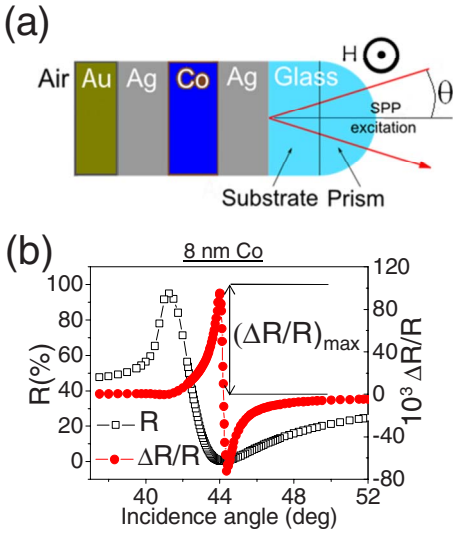

FIG. 6. (Color online) (a) Schematic view of the measurement configuration, allowing SPP excitation if light is incident from the prism side at the appropriate angle (Kretschmann configuration). (b) Measurements of the R and transverse MO Kerr effect signal (ΔR/R) for the 8 nm Co thickness sample.

model is not valid. Taking into account this fact we have simulated the effect of having a layer of Ag with large Co inclusions while keeping the same nominal Co amount. The result is a much more defined dip at around 3.7 eV (see inset in Fig. 5) which corresponds pretty well with the location of the experimentally observed dip. On the other hand the value of the Kerr rotation in the visible range is hardly affected.

Therefore we can conclude that the dip in the rotation observed at energies between 3.5 and 4 eV for the 2 and 5 nm Co sample is due to the bulk plasmon resonance of Ag since at such small Co thicknesses it is likely to have a not totally continuous Co film. This is supported by the disappearance of the dip upon increasing the nominal Co thickness.

B. Intertwined MO and plasmonic effects

In what follows, the analysis of the MO activity of the Au/Ag/Co/Ag multilayers upon SPP excitation is presented, followed by the study of the modification of the SPP wavevector when a magnetic field is applied. We present our experimental results and compare them with theoretical calculations using the optical and MO constants determined in the previous section. All this analysis is carried out in the transverse magnetic configuration that was detailed in Sec. II above.

1. Surface plasmon resonance effects on the MO activity

To study this first point, measurements of the transverse MO Kerr effect were carried out with and without SPP excitation. To excite the SPP we use the Kretschmann configuration[28] [see Fig. 6(a)]. When the reference value of the transverse MO Kerr signal without SPP excitation is needed, the measurement is performed with light coming

from the air side, incoming from the left in Fig. 6(a), where SPP excitation is not allowed.

In Fig. 6(b) we show the reflectivity versus incidence angle curve for the 8 nm Co sample as an example, together with the transverse Kerr signal ($\Delta R/R$). The SPP excitation manifests itself as a minimum on the reflectivity at a specific angle of incidence ($\theta_{min} \cong 44°$ here) above the critical angle for total internal reflection (around 41° in this case). The angle for SPP excitation corresponds to the matching between the in-plane component of the wavevector of the incident light and that of the SPP so the SPP wavevector (k_{SPP}) can be obtained from

$$k_{SPP} = \frac{2\pi}{\lambda}\sin(\theta_{min}), \tag{2}$$

where λ is the wavelength of the incident light in vacuum.

The variation in reflectivity when applying opposite magnetic fields (ΔR) also exhibits a maximum in this angular region thus the transverse Kerr signal is characterized by a sharp resonancelike angular behavior at around 44°, i.e., when the SPP is excited [Fig. 6(b)]. When the SPP is not excited [illuminating the structure from the left-hand side in Fig. 6(a), data not shown here] both R and $\Delta R/R$ basically do not exhibit any angular dependence. It has previously been shown that the values for $\Delta R/R$ in Au/Co/Au under SPP excitation conditions are one order of magnitude larger than those without SPP excitation[16,19] due both to a simultaneous reduction in the reflectivity of the system and to an enhancement of the electromagnetic field at the MO active layer, i.e., the Co layer. For the specific case of 5 nm Au/5 nm Ag/8 nm Co/7 nm Ag, shown in Fig. 6(b), we obtain a 150 times enhancement of $\Delta R/R$.

We have carried out a systematic study of the $\Delta R/R$ enhancement as a function of Co thickness in the series of Au/Ag/Co/Ag fabricated structures. Figure 7(a) shows a compilation of the $\Delta R/R$ versus incidence angle as a function of Co thickness. The characteristic resonancelike shape is observed for all Co thickness with a clear maximum in amplitude for 8 nm Co. By defining the maximum of the reflectivity variation, $(\Delta R/R)_{Max}$, as its maximum positive value [see Fig. 6(b)] we can quantify this magnitude, analyze it as a function of Co thickness, and compare it with the measured $\Delta R/R$ in the absence of SPP excitation. The results are presented in Fig. 7(b) together with the theoretically calculated values obtained using the optical and MO constants determined in the previous section. As it can be observed, when no SPP excitation is present, the MO signal exhibits the expected monotonous increase with Co thickness, with very similar experimental and theoretical values. This is in contrast with the already mentioned behavior when the SPP resonance is excited, where a maximum is observed at around 8 nm (experiments) and 6.5 nm (simulations) Co thickness, gradually decreasing for thicker Co layers. This behavior has been previously observed in Au/Co/Au (Ref. 16) and Pt-capped Ag/Co/Ag structures[27] and is due to the optimum excitation of the SPP at a specific Co thickness and the subsequent maximization of the electromagnetic field at the MO active (Co) layer for that thickness, therefore optimizing the enhancement of the MO activity. For higher Co thickness, the higher optical absorption of the system makes the damping to dominate preventing an optimal SPP excitation, leading to a reduction in the observed MO signal. As it can be seen in Fig. 7(b), the position of the maximum in the theoretically determined $(\Delta R/R)_{Max}$ differs about 1.5 nm from the experimental one. Both deviations of the actual Co thickness with respect to the nominal one and the intrinsic interface roughness present in the actual structures, may be responsible for this difference.

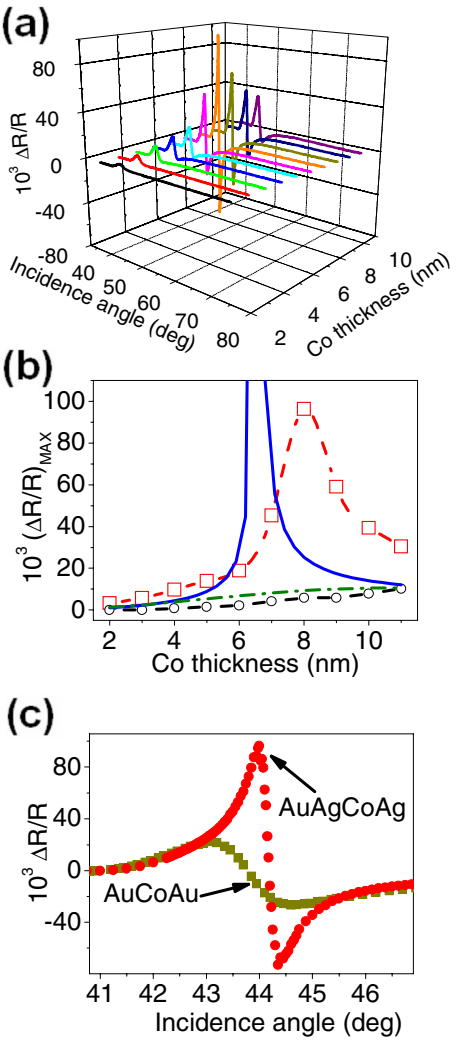

FIG. 7. (Color online) Co thickness dependence of the transversal MO Kerr signal ($\Delta R/R$). (a) Experimental $\Delta R/R$ versus incidence angle curves for different Co thickness upon SPP excitation. (b) Co thickness dependence of the $(\Delta R/R)_{Max}$, obtained both experimentally (lines with open symbols) and from simulations (lines). The continuous blue line and the dashed red line with squares correspond to the $\Delta R/R_{Max}$ values upon SPP excitation, whereas the dashed-pointed green line and the dashed black line with circles correspond to $(\Delta R/R)_{Max}$ values multiplied by ten times without SPP excitation. (c) Comparison between Au/Co/Au (squares) and Au/Ag/Co/Ag (circles) structures. The Au/Co/Au curve comes from Ref. 16. In both multilayers, the nominal Co thickness corresponds to the case of maximum SPP excitation and thus maximum $\Delta R/R_{Max}$ (5.5 nm Co for Au/Co/Au and 8 nm for Au/Ag/Co/Ag).

The observed MO enhancement in the Ag/Co/Ag can be compared with that previously obtained in the Au/Co/Au system,[16] exploring the effect of the substitution of Au by Ag and its associated improvement of plasmonic properties. In Fig. 7(c) we show $\Delta R/R$ versus incidence angle curves for optimum SPP excitation in both systems, i.e., 8 nm Co for the Au/Ag/Co/Ag structure and 5.5 nm Co for the Au/Co/Au.[16] Not only the value of $(\Delta R/R)_{Max}$ is a factor of 5 larger in the Ag/Co/Ag structure compared to the Au/Co/Au one, (10^{-1} vs 2×10^{-2}) but also the slope of the resonance in the area of SPP excitation is 20 times larger. This is due to the sharper plasmon resonance of Ag compared to Au, which comes from more negative real part of the dielectric constant of Ag at the working wavelength (633 nm).[1] This bigger slope has specially relevance in the MO surface-plasmon resonance sensing applications,[6] where the slope of the resonance is the relevant parameter that may lead to enhanced sensitivity of the device.

2. Magnetic modulation of the SPP resonance

So far we have discussed the effects that plasmon resonances can play in the MO activity of structures where materials with good plasmonic and magnetic properties coexist. Due to the presence of the magnetic layer, the optical properties of this system no longer correspond to an isotropic system but to an anisotropic one which has to be described by a dielectric tensor with nonzero off diagonal components. It is known that the dispersion relation of SPP for anisotropic media also depends on these nondiagonal elements of the dielectric matrix.[17] Since for ferromagnetic metals these elements depend on the magnetization, the application of an external magnetic field can produce a modulation in the SPP wavevector. This modulation has also been recently observed in complex Au/Co/Au structures,[16] where the ferromagnetic material present in the structures contributes with large nondiagonal elements due to its MO activity, and therefore to a sizable modulation of the SPP wavevector at low magnetic fields.

An analytical expression for the SPP wavevector modulation in those complex structures cannot be obtained but a reasonable approximation can be reached when considering a very simple system consisting of a dielectric, a thin layer of ferromagnetic material, and a very thick layer of noble metal. Assuming that the MO element ε_{xz} at saturation is much smaller than ε_{xx}, it is possible to obtain the modification of the plasmon wavevector k_{SPP} to the first order in ε_{xz} as

$$\pm\Delta k_{SPP} \equiv k_{SPP}(\pm H) - k_{SPP}(0) = \frac{i2d(\varepsilon_d\varepsilon_m)^2}{(\varepsilon_d+\varepsilon_m)(\varepsilon_d^2-\varepsilon_m^2)}\left(\frac{2\pi}{\lambda}\right)^2\left(\pm\frac{\varepsilon_{xz}}{\varepsilon_{xx}}\right). \quad (3)$$

where ε_m and ε_d are the diagonal elements of the dielectric tensor of the noble metal and the dielectric material, respectively. From this expression it is readily seen that the magnitude of the SPP modulation depends linearly on the values of the nondiagonal elements of the dielectric tensor and on the film thickness.

The analytical expression provided in Eq. (3) gives an estimation on the order of magnitude of the modulation for the SPP wavevector in our multilayered system. However an exact way to obtain the values is to employ the transfer-matrix formalism to calculate the reflectivity versus incidence angle curves with the sample magnetization saturated along opposite directions and then the variations in the reflectivity minima will provide us the SPP wavevector modulation. Figure 8(a) shows the simulated reflectivity curves for 5nmAu/5nmAg/7nmCo/7nmAg/Glass structure at $\lambda=633$ nm. The simulations exhibit an angular shift of the position of the minima due to the magnetic field, being the angular shift $\Delta\theta=\theta_{min}(H_+)-\theta_{min}(H_-)$ on the order of 10^{-2} degrees. Due to the small $\Delta\theta$ values, it is possible to

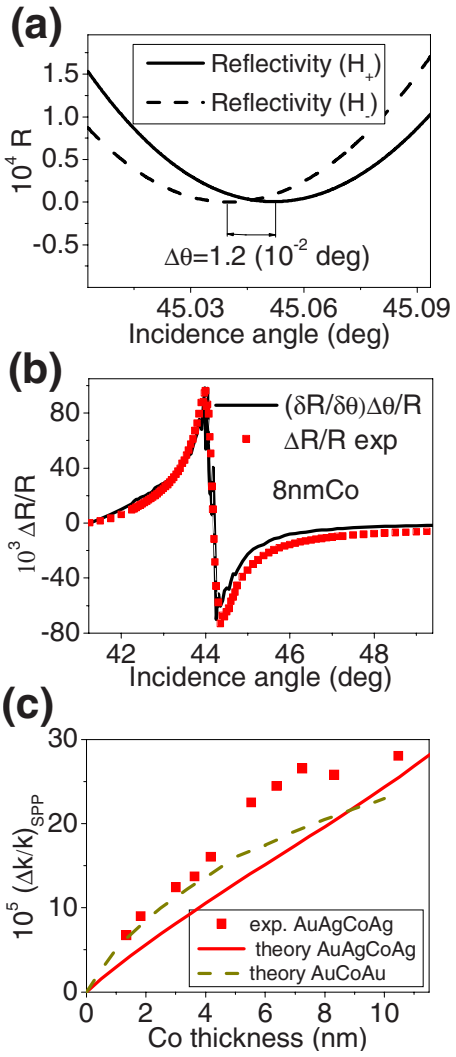

FIG. 8. (Color online) (a) Simulated reflectivity versus angle of incidence curves obtained for the sample 5nmAu/5nmAg/7nmCo/7nmAg/Glass with the magnetization saturated in one direction $\theta_{min}(H_+)$ (continuous line) and in the opposite direction $\theta_{min}(H_-)$ (dashed line). The angular shift due to the magnetic field modulation, $\Delta\theta=\theta_{min}(H_+)-\theta_{min}(H_-)$, is shown. (b) Angular derivative of the experimental reflectivity curve divided by the reflectivity and times $\Delta\theta$ [i.e., $(\delta R/\delta\theta)\Delta\theta/R$] compared with the experimental transverse MO Kerr signal ($\Delta R/R$). $\Delta\theta$ is the only fitting parameter. (c) Co thickness dependence of the $(\Delta k/k)_{SPP}$ experimental (points) and simulated (line) values. The dashed line corresponds to the simulation with the Au/Co/Au structure.

relate them with the values of Δk_{SPP} by means of the angular derivative of Eq. (2) when the angle of incidence is θ_{min}

$$\left(\frac{\Delta k}{k}\right)_{SPP} = \cot(\theta_{min})\Delta\theta. \quad (4)$$

Since the limited angular resolution of our experimental setup does not allow us to have direct access to the actual $\Delta\theta$ values, we then compare the experimental $\Delta R/R$ versus incidence angle curves with the angular derivatives of reflectivity normalized to the reflectivity $[(\delta R/\delta\theta)/R]$. In Fig. 8(b) we show these two magnitudes for the 8-nm-thick Co layer, which exhibit a very close agreement both in shape and in intensity. The proportionality factor between $\Delta R/R$ and $(\delta R/\delta\theta)/R$, taken as a parameter to adjust the amplitude of the curves, corresponds to $\Delta\theta$, which in this way can be experimentally determined. In this case, the obtained value is $\Delta\theta = 1.55(10^{-2}$ deg).

We can now explore the evolution of the magnitude of the magnetic modulation of the SPP wavevector as a function of the Co thickness for the different fabricated structures. In Fig. 8(c) we show the experimental and theoretical values of $(\Delta k/k)_{SPP}$ for our Au/Ag/Co/Ag structures as a function of the Co thickness, together with those for a Au/Co/Au as in Ref. 16. A monotonous increase in $(\Delta k/k)_{SPP}$ with Co thickness is observed in both cases, with similar experimental and theoretical values, reaching a similar modulation value of 2.8×10^{-4} for the maximum Co thickness (11 nm) for both Au- and Ag-based structures. This indicates that within the experimental conditions the main responsible for the SPP wavevector modulation is the magnetic material. Then again, being Ag a metal with smaller absorption that Au and therefore providing longer propagation distances, and since both metals confer a similar modulation potential, the use of Ag in the development of active plasmonic devices based on magnetoplasmonic systems appears to be a better option.

However, even within the simplest approximation given by Eq. (3), the modulation of the wavevector depends on the spectral dependence of the refractive index of the noble metal, the ferromagnetic metal, and the dielectric environment. Thus it would be interesting to explore the modulation considering different ferromagnetic components, such as Fe or Ni, as well as spectral dependences in future works.

IV. CONCLUSIONS

We have studied the effects of SPP excitation on the magneto-optical activity of Ag/Co/Ag trilayers as a function of Co thickness and compared them with previous results for the Au/Co/Au system. With SPP excitation, the MO transverse Kerr signal is 150 times larger when comparing with no SPP excitation for Ag/Co/Ag. This increase is associated with the enhancement of the electromagnetic field inside the Co layer due to the SPP. Moreover, the MO transverse Kerr signal enhancement is five times larger in the Ag/Co/Ag system than in the Au/Co/Au one. This is due to the lower optical absorption in the studied range and the sharper plasmon resonance of Ag versus Au. SPP wavevector modulation $(\Delta k/k)_{SPP}$ is also studied for these trilayers obtaining values on the order of 10^{-4}, similar to those obtained for Au-based structures, which pinpoints the important role of the magnetic layer on the SPP wave-vector modulation.

ACKNOWLEDGMENTS

Financial support from the Spanish MICINN ("MAGPLAS" Grants No. MAT2008-06765-C02-01/NAN and No. NAN2004-09195-C04-02, Funcoat Consolider Ingenio Grant No. 2010 CSD2008-00023) Comunidad de Madrid (References No. S-0505/MAT/0194 and No. S-0505/TIC/0191), CSIC (E. Ferreiro-Vila acknowledges JAE) and (Reference No. 2005MX0040), and European Comission (Grant No. NMP3-SL-2008-214107-Nanomagma) is acknowledged. Authors are grateful to D. Ramírez y G. Ramírez for technical assistance. This work was partially supported by CONACYT-México under Grants No. 48300 S-3907 and No. J110.474/2006 S-3904.

[1] J. R. Sambles, G. W. Bradbery, and F. Yang, Contemp. Phys. **32**, 173 (1991).
[2] H. Raether, *Surface Plasmons on Smooth and Rough Surfaces and on Gratings*, Springer Tracts in Modern Physics, Vol. 111 (Springer-Verlag, Berlin, 1988).
[3] S. A. Maier, *Plasmonics: Fundamentals and Applications* (Springer, Berlin, 2007).
[4] J. Homola, Chem. Rev. **108**, 462 (2008).
[5] J. N. Anker, W. P. Hall, O. Lyandres, N. C. Shah, J. Zhao, and R. P. Van Duyne, Nature Mater. **7**, 442 (2008).
[6] B. Sepúlveda, A. Calle, L. M. Lechuga, and G. Armelles, Opt. Lett. **31**, 1085 (2006).
[7] J.-C. Weeber, Y. Lacroute, and A. Dereux, Phys. Rev. B **68**, 115401 (2003).
[8] B. Steinberger, A. Hohenau, H. Ditlbacher, A. L. Stepanov, A. Drezet, F. R. Aussenegg, A. Leitner, and J. R. Krenn, Appl. Phys. Lett. **88**, 094104 (2006).
[9] S. I. Bozhevolnyi, V. S. Volkov, E. Devaux, J. Y. Laluet, and T. W. Ebbesen, Nature (London) **440**, 508 (2006).
[10] I. I. Smolyaninov, J. Elliott, A. V. Zayats, and C. C. Davis, Phys. Rev. Lett. **94**, 057401 (2005).
[11] Z. Liu, S. Durant, H. Lee, Y. Pikus, N. Fang, Y. Xiong, C. Sun, and X. Zhang, Nano Lett. **7**, 403 (2007).
[12] T. Nikolajsen, K. Leosson, and S. I. Bozhevolnyi, Appl. Phys. Lett. **85**, 5833 (2004).
[13] J. Gómez Rivas, J. A. Sánchez-Gil, M. Kuttge, P. H. Bolivar, and H. Kurz, Phys. Rev. B **74**, 245324 (2006).
[14] D. Pacifici, H. J. Lezec, and H. A. Atwater, Nat. Photonics **1**, 402 (2007).
[15] B. Sepúlveda, L. M. Lechuga, and G. Armelles, J. Lightwave Technol. **24**, 945 (2006).
[16] J. B. González-Díaz, A. García-Martín, G. Armelles, J. M. García-Martín, C. Clavero, A. Cebollada, R. A. Lukaszew, J. R. Skuza, D. P. Kumah, and R. Clarke, Phys. Rev. B **76**, 153402

(2007).
[17] R. F. Wallis, J. J. Brion, E. Burstein, and A. Hartstein, Phys. Rev. B **9**, 3424 (1974).
[18] N. Bonod, R. Reinisch, E. Popov, and M. Nevière, J. Opt. Soc. Am. B **21**, 791 (2004).
[19] V. I. Safarov, V. A. Kosobukin, C. Hermann, G. Lampel, J. Peretti, and C. Marlière, Phys. Rev. Lett. **73**, 3584 (1994).
[20] C. Hermann, V. A. Kosobukin, G. Lampel, J. Peretti, V. I. Safarov, and P. Bertrand, Phys. Rev. B **64**, 235422 (2001).
[21] L. Sapienza and D. Zerulla, Phys. Rev. B **79**, 033407 (2009).
[22] G. Armelles, J. B. González-Díaz, A. García-Martín, J. M. García-Martín, A. Cebollada, M. U. González, S. Acimovic, J. Cesario, R. Quidant, and G. Badenes, Opt. Express **16**, 16104 (2008).
[23] P. B. Johnson and R. W. Christy, Phys. Rev. B **6**, 4370 (1972).
[24] L. Novotny and B. Hetch, *Principles of Nano-Optics* (Cambridge University Press, Cambridge, 2006), pp. 391–392.
[25] G. J. Kovacs, Surf. Sci. Lett. **78**, L245 (1978).
[26] S. Szunerits, X. Castel, and R. Boukherroub, J. Phys. Chem. C **112**, 15813 (2008).
[27] E. Ferreiro-Vila, X. M. Bendana Sueiro, J. B. Gonzalez-Diaz, A. Garcia-Martin, J. M. Garcia-Martin, A. Cebollada Navarro, G. Armelles Reig, D. Meneses Rodriguez, and E. Munoz Sandoval, IEEE Trans. Magn. **44**, 3303 (2008).
[28] E. Kretschmann and H. Raether, Z. Naturforsch. A **23**, 2135 (1968); E. Kretschmann, Z. Phys. **241**, 313 (1971).
[29] W. S. Kim, M. Aderholz, and W. Kleemann, Meas. Sci. Technol. **4**, 1275 (1993).